The impact of syn-faulting porosity reduction on damage zone architecture in porous sandstone: an outcrop example from the Moab Fault, Utah

Tord Erlend Skeie Johansen*, Haakon Fossen, Richard Kluge

Department of Earth Sciences, University of Bergen, Allégt. 41, N-5007 Bergen, Norway

Abstract

Deformation structures in the Jurassic Moab Member of the Entrada Sandstone have been studied in the Courthouse area where two major fault segments (Segments A and B) of the Moab Fault are connected. Field data show that Segment A developed from an early stage of (thick) deformation band formation and that distinctively thinner deformation bands and fractures were subsequently added to its damage zone at a later stage. Only the second stage is expressed along Segment B. Geometric and kinematic evidence indicates that Segment B linked with Segment A at the time when Segment A (and its thick deformation bands) was already present in the Courthouse area. We attribute the transition from thick deformation bands to thin deformation bands to pore-space reduction caused by syn-faulting quartz dissolution and precipitation that changed the mechanical properties of the rock. In this model, thin deformation bands formed as porosity was reduced during quartz diagenesis. The observations underscore the importance of syn-kinematic diagenetic changes and the variation in small-scale structures along faults that apparently formed during the same faulting event in porous sandstones.
© 2005 Elsevier Ltd. All rights reserved.

Keywords: Fault architecture; Fault damage zone; Fault branch point; Deformation band; Quartz diagenesis

1. Introduction

Small-scale structures associated with faults have attracted increasing attention over the past few decades, both for academic and petroleum-economic reasons (Aydin and Johnson, 1978; Underhill and Woodcock, 1987; Antonellini and Aydin, 1994; Fowles and Burley, 1994; Fossen and Hesthammer, 1997; Hesthammer and Fossen, 2000; Shipton and Cowie, 2003). In this context, the relationship between the various types of deformation bands and fractures, as well as where and when they form is of interest. In general, deformation bands form in porous rocks and in sediments such as porous sands and volcanic deposits (Dunn et al., 1973; Mair et al., 2000; Wilson et al., 2003), whereas small-scale fractures form in non-porous or low-porous rocks such as limestones and well-cemented sandstones.

Aydin and Johnson (1978) presented field evidence that the formation of faults (slip surfaces) in sandstones is preceded by extensive development of deformation bands and related collapse of pore space. On the other hand, in low-porous rocks, faults grow from formation and linkage of microcracks (Reches and Lockner, 1994). One of the current challenges is to identify the conditions that favor deformation band growth versus fracturing. A second challenge is to understand the controls on the formation of different types of deformation bands. Different types of deformation bands include various classes of cataclastic bands (Aydin, 1978), compaction bands (Mollema and Antonellini, 1996), dilation bands (Du Bernard et al., 2002), framework phyllosilicate bands (Knipe et al., 1997) and cemented or diagenetically altered bands (Hesthammer et al., 2002). The various factors influencing the type of deformation band product as well as formation of fractures versus deformation bands have not yet been constrained.

The current contribution presents data from a fault branch area where two large fault segments interact. The outcrop is studied in detail, and a history is outlined where thick cataclastic deformation bands are succeeded by the formation of unusually thin deformation bands with slip

---

* Corresponding author. Tel.: +47 55 58 33 60; fax: +47 55 58 36 60.
E-mail address: tord.johansen@geo.uib.no (T.E.S. Johansen).

surfaces. In this case the different structures have developed in the same sandstone, at more or less the same burial depth during the evolution of a single set of faults in a rock that experienced porosity reduction by quartz dissolution and cementation simultaneously with faulting.

2. Geological setting

2.1. Regional geological framework

The study area (Fig. 1) is located on the Colorado Plateau in east-central Utah, along US highway 191, about 30 km north of the town of Moab. Structurally, this part of the Colorado Plateau is located in the Paradox Basin and features several salt cored anticlines and normal faults.

Thick salt beds were deposited in the Paradox Basin during the Pennsylvanian. Subsidence and initial salt movement commenced in the Permian and continued until the Early Jurassic. Large salt diapirs developed above NW-trending Proterozoic basement fault lineaments (Stevenson and Baars, 1986; Doelling, 1988). Renewed salt movement in the Late Cretaceous continued throughout the Tertiary, associated with development of large faults, such as the Moab Fault, along the crest of the salt cored anticlines (Doelling, 1988; Foxford et al., 1996). Deformed Quaternary deposits within the Arches National Park indicate that salt diapirism is currently active (Oviatt, 1988). Salt dissolution and collapse of overlying strata associated with the Late Tertiary exhumation of the Colorado Plateau has also contributed to the structuring of the area (Huntoon, 1988).

2.2. Stratigraphy

The stratigraphy of the study area has been reviewed in detail by Foxford et al. (1996) and is consistent with that of the Arches National Park to the east (Doelling, 1988). A summary of stratigraphic key units to this study (Fig. 2) is presented here.

Outcrops in the study area show thick beds of Jurassic eolian sandstones. The Middle Jurassic Entrada Formation is represented by the Slick Rock Member, which is a generally fine-grained sandstone containing some scattered medium to coarse cross-beds. The Moab Member was previously considered to represent a tongue of the Entrada Formation, but has recently been reassigned to the overlying Curtis Formation (Doelling, 2000). The Moab Member is a pale-yellow-brown, fine- to medium-grained, massive and well-indurated quartz arenite, typically with large low-angle cross-beds, and forms a resistant cap over the underlying rock units. In the Courthouse area the thickness of the Moab Member is about 28 m (Foxford et al., 1996).

The porosity of the Moab Member is generally high, in the range of 20–25% (Antonellini and Aydin, 1994), but is locally less than 1% in the Courthouse area. Footwall exposures reveal a few-meter-thick sandy siltstone at the contact between the Moab Member and the Slickrock Member. This silt unit has been correlated with the Curtis Formation in the San Rafael Swell to the west (O'Sullivan, 1981). The Morrison Formation rests on the Moab Member and includes flood plain and fluvially deposited mudstones, siltstones, and sandstones. Strata in the immediate hanging wall of the Moab Fault belong to the Early Cretaceous
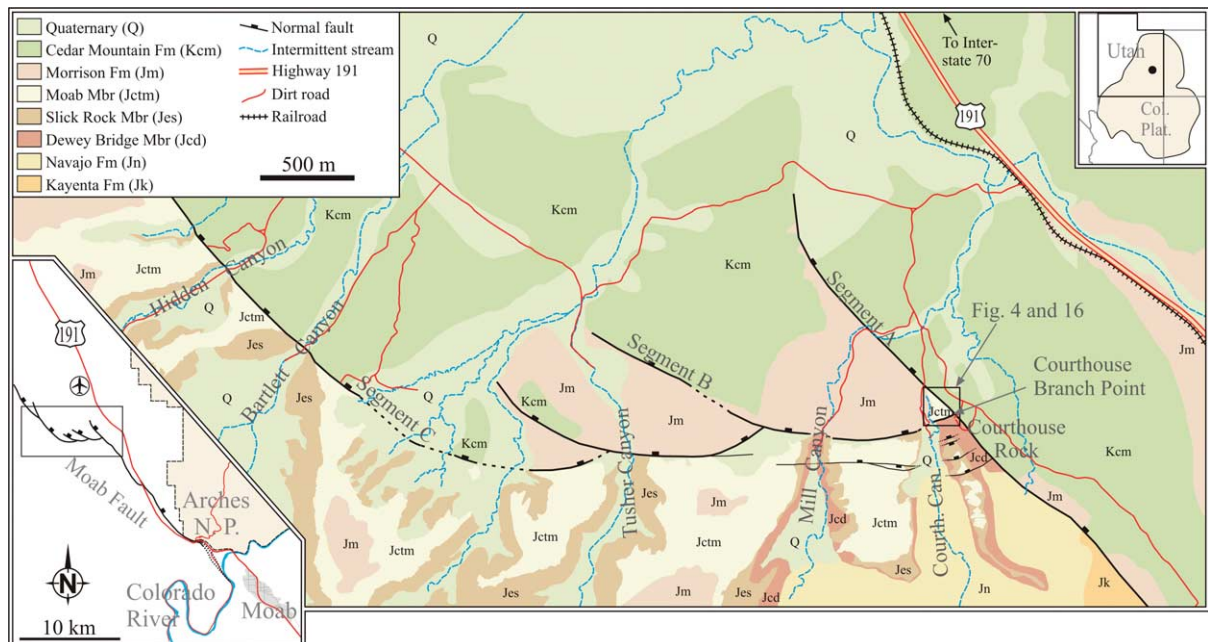

Fig. 1. Index map of the study area and the Moab Fault. Modified from Doelling (2001). The fault strands have been named according to Foxford et al. (1996).
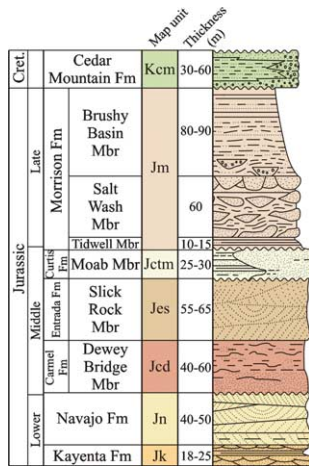
Fig. 2. Stratigraphy of the study area. Modified from Doelling (2001).

Cedar Mountain Formation and include shale, sandstone, conglomerate, and minor limestone.

2.3. The Moab Fault

The Moab Fault (Fig. 1) is one of several large NW-striking salt-related structures that developed in concert with Late Cretaceous and Tertiary salt movement, and it is assumed to extend into the underlying salt beds of the Paradox Formation (Doelling, 1988, 2001). Its maximum throw is about 950 m near the Arches National Park entrance area, and its total length in outcrop is about 45 km (Foxford et al., 1996). In the study area, the Moab Fault is composed of a series of west-stepping, hard-linked fault strands. Two of these strands, here referred to as Segments A and B (Fig. 1, terminology from Foxford et al. (1996)), were studied.

Segment A, which is the largest segment of the Moab Fault, defines a structure that is over 20 km long and continues southeast toward the Moab Valley. To the north Segment A terminates about 1.5 km northwest of the Courthouse Branch Point, where it bends toward the hanging wall side. The throw is approximately 200 m in the Courthouse Rock area.

The 2–2.5-km-long Segment B exhibits a near-linear NW-oriented surface trace along its westernmost section, but the east section gradually curves toward and hard-links with Segment A at a 60° angle. This hard-link structure is referred to as the Courthouse Branch Point (Foxford et al., 1996). The throw across Segment B close to the Courthouse Branch Point is about 80–90 m, but increases toward the Mill Canyon area.

Regional sub-vertical joints, associated with Tertiary uplift and erosion (Foxford et al., 1996), are well expressed in the Moab Member west of the Moab Fault and are comparable with those studied in the Arches area (Cruikshank et al., 1991; Zhao and Johnson, 1992). These

joints have not been observed in the currently examined outcrop.

Reconstruction of the burial history of the Jurassic sand units adjacent to the Moab Fault suggests that fault-related deformation occurred at the maximum depth of burial of about 2 km (Garden et al., 2001). The burial depth remained more or less constant throughout the deformation. Corresponding temperatures in the Jurassic sands have been estimated at approximately 80 °C (Nuccio and Condon, 1996; Garden et al., 2001).

3. Methodology

Field mapping was restricted to the homogeneous eolian sandstone unit of the Moab Member. Sparse vegetation and sediment cover provide excellent lateral exposure, facilitating sampling of high-resolution field data from scan-line profiles and 2D surface grids. The stratigraphic and structural framework was mapped from digital high resolution (1×1 m) orthorectified aerial photos. Plane orientation data follows the right hand rule throughout this paper.

Hand specimens were sampled at different positions on the outcrop and prepared for thin section. Digitized photomicrographs (8-bit color mode) captured under plain polarized light were processed and analyzed by means of conventional imaging software to quantify the 2D porosity, i.e. the cross-sectional porosity derived from a random slice through the sample (Fig. 3). We assume that the 2D porosity is approximately equal to the 3D porosity. Each sample was impregnated with blue dyed epoxy resin, facilitating discrimination of open pore space from the mineral grains. The pores are accordingly revealed as blue structures, whereas the mineral grains appear as white to light brown. The image analysis involved segmentation and conversion of the 8-bit color images to binary images. Since there is no
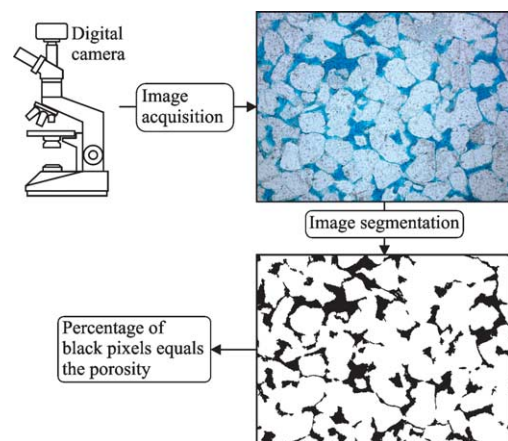

Fig. 3. Determination of porosity from digital images of thin sections under plane polarized light. Blue color represents open pore space in the unprocessed image, whereas black is assigned to open pore space in the binary image.

universal segmentation technique that will work for all images, each image had to be processed separately. Manual editing was necessary to remove unwanted features from the image and to enhance the color contrast between the pores and the mineral grains. The binary images display two contrasting colors, one representing pore space, the other representing grains and cement.

4. Courthouse branch point

4.1. Outcrop description

The Courthouse Branch Point (Fig. 4) defines the hard-link structure between Segment A and Segment B. Here, a remarkably well-exposed outcrop of the Moab Member occupies a 60° sector of the damage zone, which is bounded to the south and northeast by the respective faults. Segment B is oriented at 252/75, whereas Segment A is oriented at 313/60. The Moab Member dips gently ($\sim 5°$) toward the WNW where it subcrops beneath the Tidwell Member of the Morrison Formation. Structural lineaments on the top surface of the Moab Member were mapped from a grid of 21 scan-lines directed along the magnetic longitude and spaced 10 m apart (Fig. 4).

The microtexture of the Moab Member at the Courthouse

Branch Point locality reveals a strong diagenetic overprint dominated by quartz diagenesis and carbonate cementation. Quartz diagenesis is evident from dissolution at grain contacts (Fig. 5a) and overgrowth in open pore spaces (Fig. 5b). Quartz dissolution and overgrowth has contributed significantly to the reduction of the primary porosity of the host rock, but is not uniformly distributed across the outcrop. Current host rock porosities show significant variation within short distances and range from less that 1% (Fig. 5c) to 17% (Fig. 5d). Details on the porosity data are provided in Table 1, which also includes references to photomicrographs presented in this paper. Sample locations are shown in Fig. 4.

Table 1 also summarizes the amount of carbonate cement obtained from the thin section analysis. Our study indicates that the effect of carbonate cementation on the reduction of porosity is moderate and relatively local compared with quartz diagenesis. Carbonate cement is mainly restricted to spherical concretions as well as dilated joints and slip surfaces. Joints are locally enveloped by carbonate indurated wall-rock mantles where porosity is reduced to zero. Spherical concretions range in diameter from a few millimeters up to ~ 10 cm and become more abundant adjacent to the branch point, but also tend to cluster around fracture networks. Thin sections of these concretions (Fig. 5e) show that the pores are completely saturated
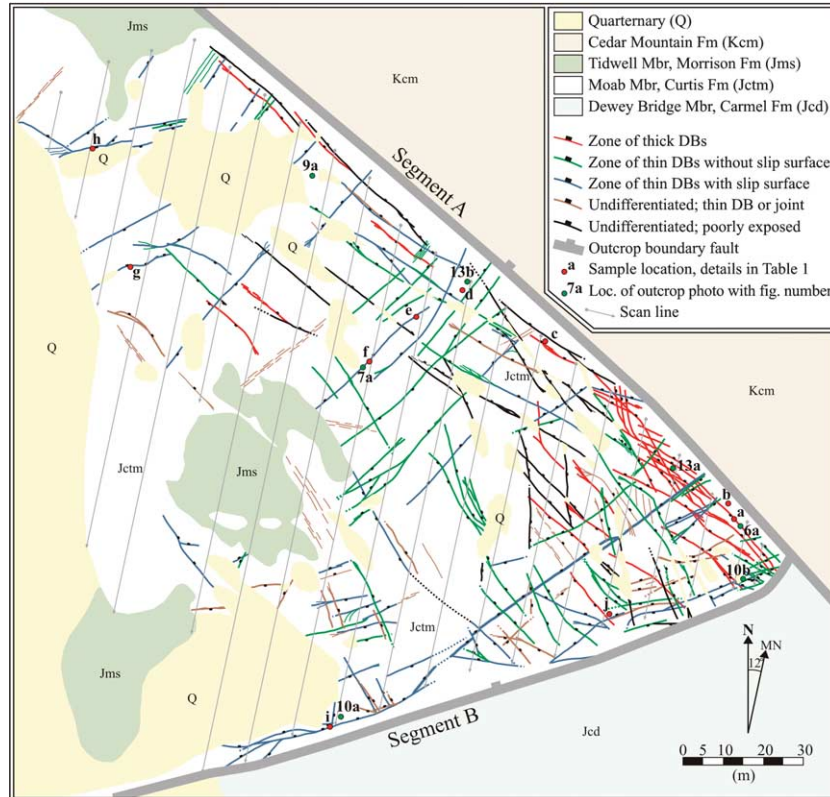

Fig. 4. Structural outline of the Courthouse Branch Point locality. Only the most laterally continuous structures are shown at this scale. Deformation bands (DBs) and slip surfaces dominate the damage zone. The presence of joints has been indicated, but not verified at the scale of mapping shown here. Thick lineaments represent zones of sub-parallel deformation structures, whereas thin lineaments represent single structures.
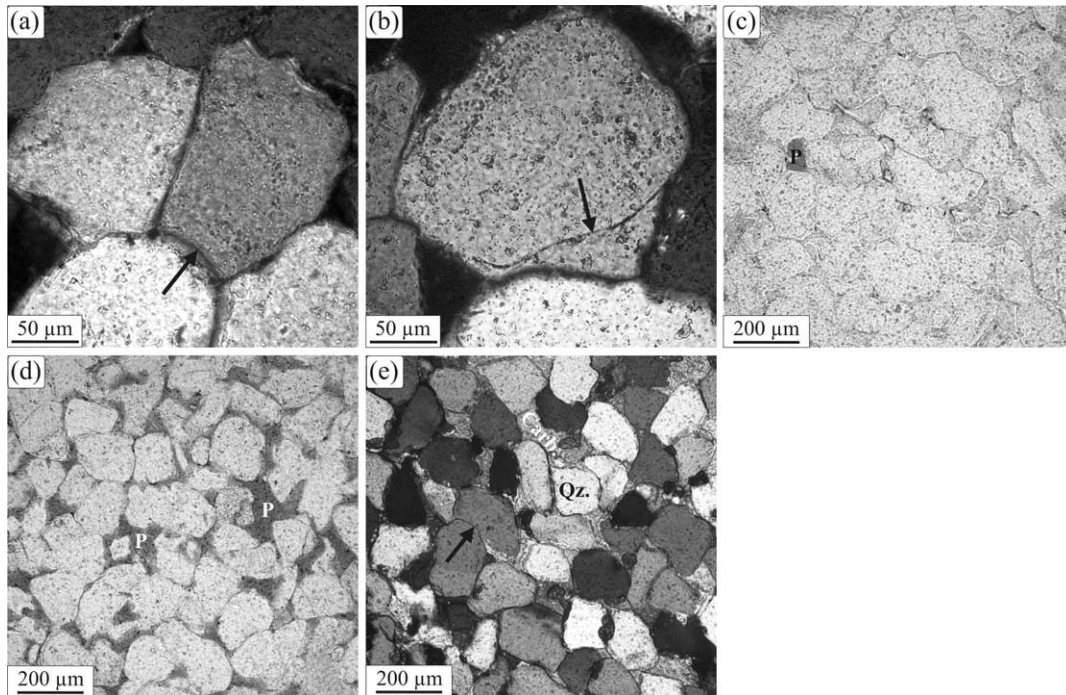
Fig. 5. Photomicrographs of the host rock (Moab Member) at the Courthouse Branch Point locality. Sample locations are listed in Table 1. (a) Quartz dissolution at grain contacts (arrow). (b) Quartz overgrowth in open pores. Note the trace of the detrital grain boundary (arrow). (c) Locally, the porosity (P) has been reduced to less than 1% due to quartz diagenesis. (d) Approximate maximum porosity (~17%) on outcrop. (e) Photomicrograph of the interior of a spherical concretion demonstrates that the pores are completely filled with carbonate cement. Evidence of quartz dissolution (arrow) is also present within the concretions.

with carbonate cement. We have not differentiated between the various types of carbonate cements, but examination of vein networks at the Courthouse Branch Point locality by Foxford et al. (1996) indicates that the carbonate is predominantly calcite.

Although limited documentation is presented here, it is conceivable that the spatial variation in porosity within the damage zone can be attributed in part to the presence of slip surfaces, capable of transmitting fluids that have interacted

with the wall-rock, or deformation bands that may have compartmentalized the fluid flow pattern.

Four types of deformation structures have been identified in the Moab Member: (1) thick deformation bands, (2) thin deformation bands, (3) slip surfaces, and (4) joints. These structures feature contrasting deformation mechanisms as well as contrasting hydrodynamic properties.

4.2. Thick deformation bands

'Thick' (~1–1.5 mm wide) deformation bands are identical to cataclastic deformation bands as described by Aydin (1978) and Fossen and Hesthammer (1997) from the San Rafael Desert, and by Antonellini and Aydin (1994) from the Arches area. The designation 'thick' is used solely to distinguish them from the thinner deformation bands described below. In outcrop the thick deformation bands exhibit a slightly paler hue compared with the host rock. They generally cluster in centimeter-wide zones comprised of 2–10 individual bands (Fig. 6a) and form a slightly raised relief in outcrop. These deformation band zones may show characteristic internal anastomosing arrangement along strike.

Photomicrographs (Fig. 6b) reveal a microstructure dominated by larger (~50–150 μm) grain fragments and scattered, undeformed quartz grains (~100–200 μm) surrounded by relatively fine-grained (<30 μm) fragments. Quartz granulation appears to be more advanced in the

Table 1
Overview of porosities and amount of carbonate cement in samples taken from the Moab Member at the Courthouse Branch Point

Sample[a]	Figures	Porosity (%)	Carbonate cement (%)
a	5c and 6c	4	<1
b	5e	~1	18
c	5a and d, 6b, and 15a	16.5	<1
d	13b	<1	6
e	–	7.2	4
f	5b, 7b and d, and 9b and c	13.5	<1
g	–	<1	3
h	7c, 8, and 15b	<1	~1
i	–	<1	20–25
j	10c	<1	20–25

Note references to photomicrographs presented in this paper.
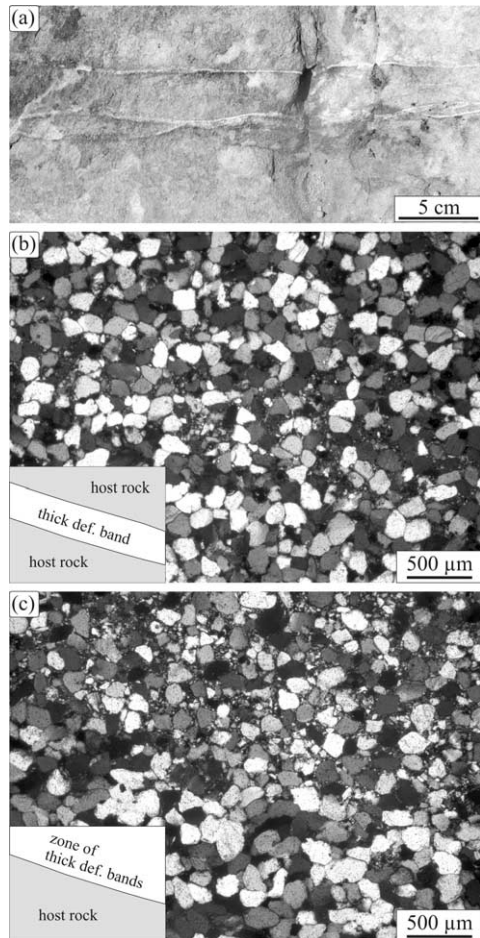[a] Sample locations are shown in Fig. 4.

Fig. 6. Thick deformation bands in the Moab Member at the Courthouse Branch Point locality. (a) Outcrop photo of an anastomosing zone of thick deformation bands. Photomicrographs (crossed polars) reveal (b) moderate cataclasis along single thick deformation band and (c) somewhat better developed cataclasis along zones of thick deformation bands. See Fig. 4 and Table 1 for location and details.

deformation band zones than in single deformation bands as a result of higher strain (Fig. 6c).

4.3. Thin deformation bands

The thin deformation bands have widths of 0.1–0.2 mm and exhibit white coloration in outcrop. Similar to the thick deformation bands, the thin deformation bands typically cluster in zones that range in width from a few millimeters to several centimeters. The thinner (<1–2 cm), more densely packed sections along these zones (Fig. 7a) commonly exhibit internal anastomosing geometries perpendicular to the slip direction, comparable with that of zones of thick deformation bands. The thicker sections, however, display more heterogeneous internal geometries where anastomosing geometries occur in alteration with more chaotic structural patterns. Anastomosing bands often confine centimeter-wide and tens of centimeter long lenses of pristine host rock, whereas the latter sections contain
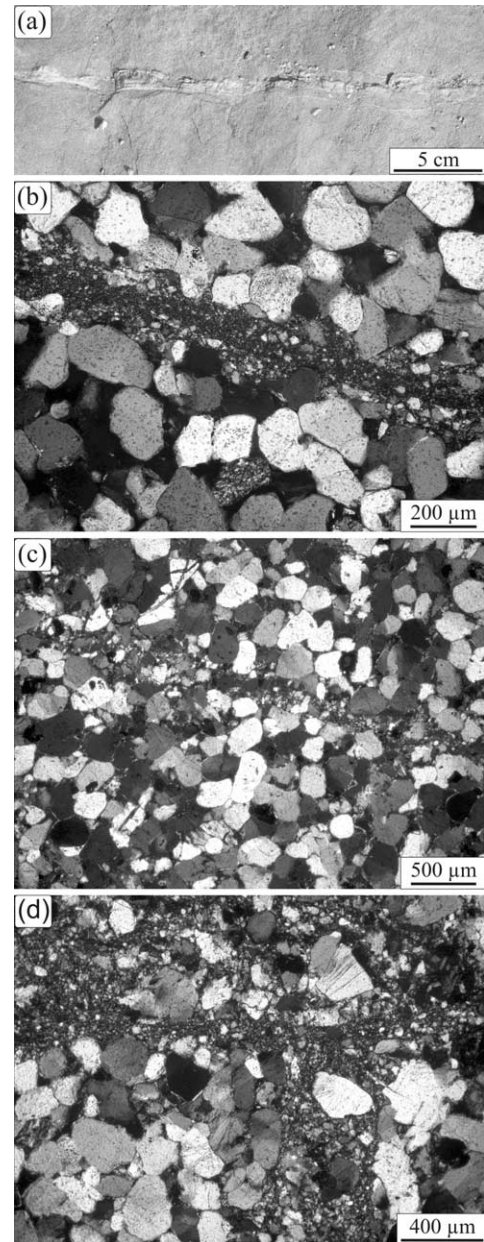

Fig. 7. Thin deformation bands in the Moab Member at the Courthouse Branch Point locality. (a) Zone of thin deformation bands with internal anastomosing geometry in outcrop. Photomicrographs showing (b) throughgoing single thin deformation band characterized by intensive localized cataclasis, (c) poorly developed single thin deformation band, and (d) a zone of thin deformation bands. The microstructure of zones of thin deformation bands is generally more heterogeneous than that of single thin deformation bands. See Fig. 4 and Table 1 for location and details.

irregularly shaped host rock pockets. In vertical sections, i.e. sections sub-parallel to the slip direction, zones of thin deformation bands appear as sub-planar.

Photomicrographs show that the thin deformation bands are clearly cataclastic structures. Coherent bands (Fig. 7b) are characterized by intense grain comminution that produces a fine-grained quartzose matrix or gouge with some scattered larger grain fragments, but with very few

undeformed quartz grains. The finest fraction of the gouge (<5 μm) typically occupies the center of the thin deformation bands and displays as dark colored matter under crossed polars. Individual grain fragments at this scale are indiscernible by conventional optical microscopy. The degree of cataclasis along the thin deformation bands appears to vary in response to the offset. Sections associated with low offset typically exhibit more moderately crushed grains and a larger number of visible angular grain fragments (Fig. 7c). The microstructure of zones of thin deformation bands is more heterogeneous compared with single thin deformation bands. In particular, coalescence of individual bands within the zones gives rise to wider cataclastic zones where grain size distribution is less systematic (Fig. 7d). Moderately deformed or undeformed microscopic lenses or pods are also preserved within these zones. Feldspar grains inside some of the lenses are more fractured than quartz grains, probably due to cleavage.

Examination of the tip region of a thin deformation band (Fig. 8) has provided useful insight into the micro-kinematics of the thin deformation bands and how the host rock accommodated initial shear movement at the time these structures formed. The offset increases from the tip line toward the central section of the band. Clast-supported gouge dominates the 1.6-mm-long and less coherent section proximal to the tip. This section characterizes the deformation product of incipient localized shear and contains a framework of larger similarly sized (50–100 μm) clasts. There is no compelling evidence for grain reorganization and dilation at the tip, indicating that the thin deformation bands nucleated ultimately by localized cataclasis. Reduction in clast size and an increase in the content of fine-grained gouge mark the formation of matrix-supported cataclasite and a more coherent band less than 2 mm away from the tip. These observations suggest that minor offset, probably much less than 0.5 mm, was required to establish a coherent thin deformation band.

Field observations suggest that the thin deformation bands are not restricted to the Moab Member fault damage zone at the Courthouse Branch Point. Similar structures have also been observed in similar lithologies that have undergone quartz diagenesis and porosity reduction else-where along the main fault strands. Here, however, the thin deformation bands occur preferentially close to the fault core and do not constitute a major portion of the fault damage zone.

4.4. Slip surfaces

Outcropping slip surfaces commonly appear as smooth, locally polished fractures that feature a planar to slightly corrugated morphology along strike. Striation marks are common (Fig. 9a) and vertical exposures may reveal offset of bedding laminations within the Moab Member. All of the slip surfaces were associated with zones of sub-parallel thin deformation bands. Slip surfaces have not been observed in
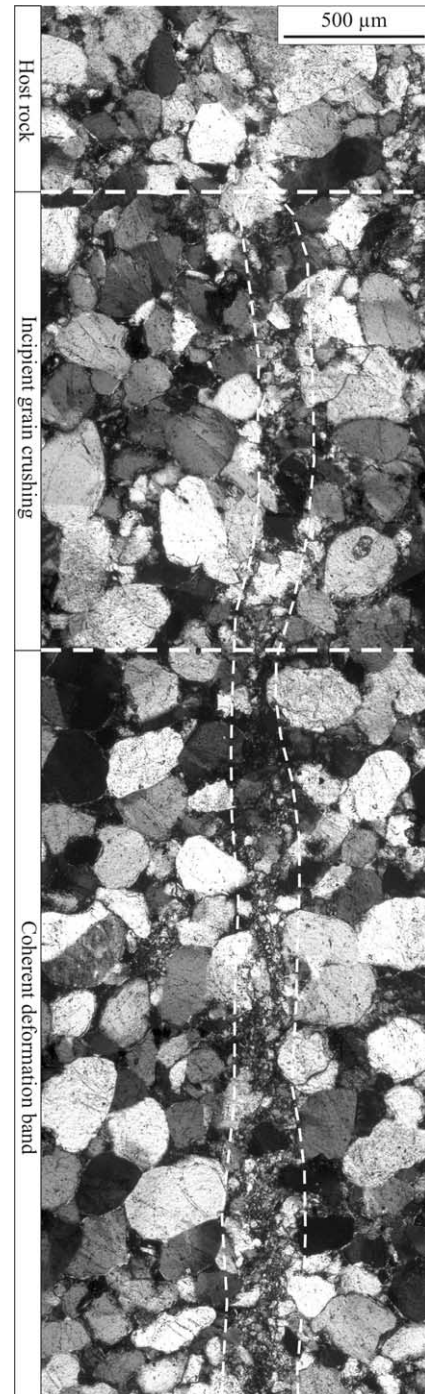

Fig. 8. The microstructure of the tip of a thin deformation band reveals that these structures develop ultimately by cataclasis. Sample location is listed in Table 1.

association with the thick deformation bands, but these structures may coexist closer to the less exposed fault core of Segment A, where strain is higher.

Thin sections reveal continuous microscopic fractures within single thin deformation bands and zones of thin deformation bands (Fig. 9b). These structures form near-planar rock discontinuities that locally cut off grain
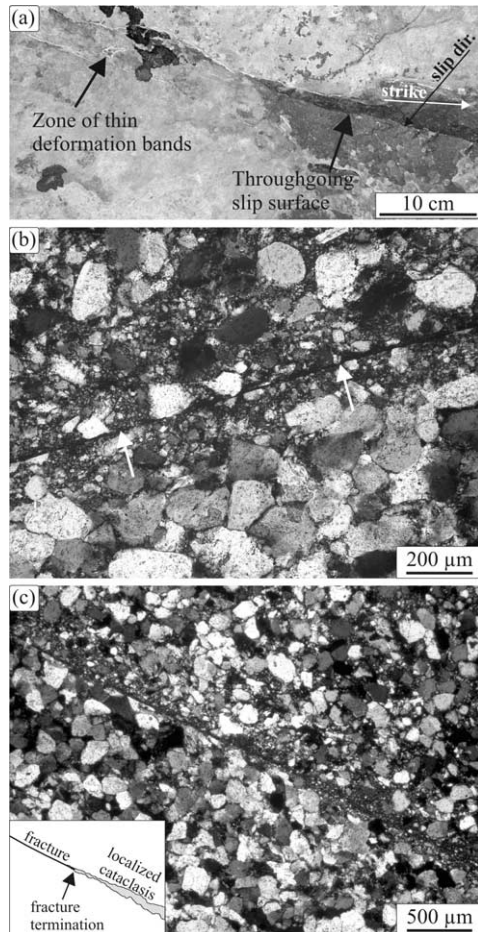
Fig. 9. Slip surfaces associated with thin deformation bands in the Moab Member at the Courthouse Branch Point locality. (a) Striated slip surfaces have been frequently observed along zones of thin deformation bands in outcrop. (b) Photomicrograph showing a discrete fracture (arrows) interpreted as a slip patch inside a zone of thin deformation bands. (c) Termination of a slip patch along a zone of localized cataclasis inside a zone of thin deformation bands. See Fig. 4 and Table 1 for location and details.

fragments inside the deformation bands and grains along the rugged sidewall of the deformation bands. Local apertures on the order of 10–40 μm, often associated with carbonate fill, are common. The process zone ahead of the tip of these micro-fractures is characterized by extensive cataclasis and gouge formation internally along the thin deformation bands (Fig. 9c). The finest fraction of the gouge localizes in narrow (10–20 μm) seams that extend out from the fracture tip and may take on subtle anastomosing geometries. We suggest that these micro-fractures represent small slip patches that nucleated within the most fine-grained gouge as displacement accumulated along the thin deformation bands.

4.5. Joints

Joints are typically filled with carbonate and may have apertures up to 1 cm, although apertures of less than 1 mm are most common. Most of the joints are enveloped by a millimeter- or centimeter-wide zone of calcite indurated wall rock. The occurrence and distribution of joints across the Moab Member outcrop is somewhat ambiguous, as there are few distinctive features that can be used to discern joints from thin deformation bands and associated slip surfaces without close examination under a magnifying lens or microscope. Abundant carbonate-filled joints have been observed in the vicinity of Segment B, where the joints cluster in highly connected networks (Fig. 10a). There are also indications of more laterally continuous joints that parallel Segment B close to the fault core (Fig. 10b).

The microstructure of the joints is characterized by rugged morphology and absence of comminuted grains (Fig. 10c), indicating that these fractures formed by opening mode failure rather than shear failure.
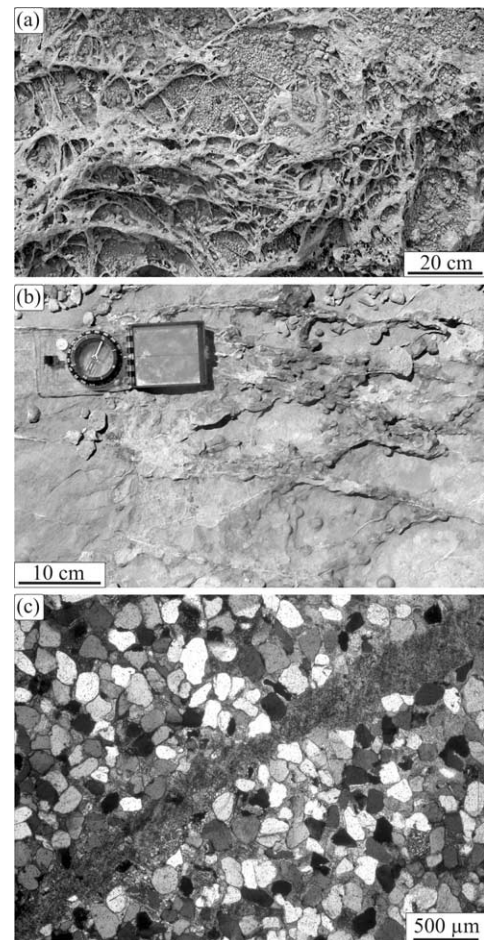

Fig. 10. Joints in the Moab Member at the Courthouse Branch Point locality. Outcrop photos showing (a) local joint networks close to Segment B and (b) joint arrays sub-parallel to Segment B. None of these structures are delineated in Fig. 4. (c) Photomicrograph of a joint. The absence of comminuted grains as well as the aperture associated with carbonate fill, show that this structure did not form through shear failure, but by opening mode failure. See Fig. 4 and Table 1 for location and details.

4.6. Orientations and sub-populations

Strike and dip orientations (right hand rule used throughout this paper) were sampled from the laterally continuous structures delineated in Fig. 3. Most of the deformation structures in the damage zone are sub-parallel to one of the main fault segments. The main dip population falls in the interval of 60–85° and displays a Gaussian distribution about a sample mean of 73° (Fig. 11). The thick deformation bands (Fig. 12a) are sub-parallel to Segment A and form two prominent sub-sets oriented at 300/73 and 136/65 (sample mean). These sets are mutually intersecting and define orthorhombic compartments in plan view. Other deformation structures within the damage zone, i.e. thin deformation bands, associated slip surfaces and joints, are grouped into seven sets. Set 1 (250/81) (Fig. 12b) dips steeply and is synthetic to Segment B, whereas set 2 (075/70) (Fig. 12c) has slightly shallower dip and is antithetic to Segment B. Sets 3 (226/80) (Fig. 12d) and 4 (045/71) (Fig. 12e) die out to the SW and form two trends of steep oppositely dipping structures that strike normal to Segment A. The strike of sets 3 and 4 does not differ significantly ($\sim$20°) from sets 1 and 2, but their spatial distribution is distinctive; sets 1 and 2 occur dominantly in the vicinity of Segment B, whereas sets 3 and 4 are widely distributed across the outcrop. Set 5 (309/72) (Fig. 12f) constitutes abundant thin deformation bands and slip surfaces dipping synthetically to Segment A. Orthorhombic compartments bounded by synthetically paired structures in set 5 are similar in plan view to the orthorhombic compartments bounded by the thick deformation bands (Fig. 9a), but the latter are bounded by antithetical structures. Set 6 (131/79) (Fig. 12 g) is antithetic to set 5 and exhibits the same type of deformation structures as set 5, although they are much less frequent. The average dip of set 6 is steeper (7°), however, this is conceivably due to layer rotation away from Segment A in connection with faulting along Segment A. Set 7 (Fig. 12h) is oriented at 348/68, oblique to both Segment B and Segment A.
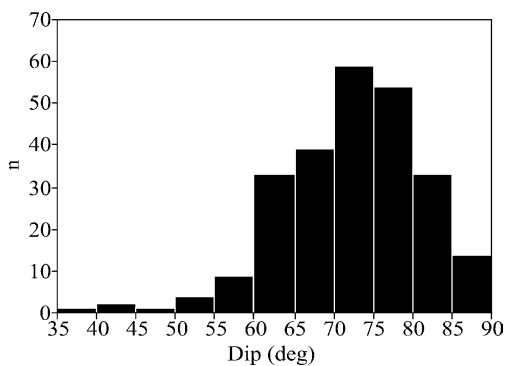

Fig. 11. Distribution of dip of deformation structures at the Courthouse Branch Point locality. The sample mean is 73°.

4.7. Relative timing of thick and thin deformation bands and joints

Constraints on the relative timing of the structures in the damage zone have been addressed by examining cross-cutting relationships. Two important findings were made. First, the thick deformation bands are overprinted by the thin deformation bands and associated slip surfaces and joints, and thus represent the oldest structures (Fig. 13a). Second, structures oriented normal to Segment A (sets 3 and 4) are offset by sets 5 and 6, oriented parallel to Segment A. Accordingly, sets 3 and 4 predates sets 5 and 6. Cross-cutting relationships between sets 1 and 2 and sets 3 and 4 have not been observed due to poor exposure in the southeast section of the outcrop. However, these two respective trends exhibit similar orientations and are therefore interpreted to have developed more or less simultaneously. Due to poor exposure, no cross-cutting relationships have been established for set 7.

Cross-cutting relationships between joints and deformation bands have not been observed in outcrop, but the photomicrograph in Fig. 13b show a carbonate filled joint that formed in carbonate cemented gouge inside a zone of thin deformation bands, suggesting that the joints post-dates formation of the deformation bands. This finding is consistent with Davatzes and Aydin (2003) and their observations of deformation bands and joints elsewhere in the Courthouse area.

4.8. Temporal relations between cements and deformation structures

Cross-cutting relationships suggest that the thick deformation bands postdate the thin deformation bands. Furthermore, it is evident that the host rock has been diagenetically altered through extensive quartz cementation/dissolution and carbonate cementation, which is related to interaction of formation waters and fluids ascending the Moab Fault (Foxford et al., 1996; Garden et al., 2001). Cementation has resulted in reduction of porosity and alteration of the mechanical property of the host rock. Based on these considerations, special attention has been paid to unravel the temporal relations between cementation and the various deformation structures at the Courthouse Branch Point outcrop. Our observations are summarized in Fig. 14.

Quartz dissolution at the contact between undeformed grains and/or larger clasts is frequently observed inside the thick deformation bands (Fig. 15a), suggesting that the thick deformation bands predate extensive quartz cementation.

The thin deformation bands appear to postdate extensive quartz diagenesis. Transgranular fractures that cut off grain dissolution interfaces in the immediate sidewalls (Fig. 15b), strongly indicates that quartz dissolution preceded cataclasis. These fractures are oriented sub-parallel to the band, suggesting that the cross-cut quartz grains did not undergo rotation and sliding and that the host rock was firmly
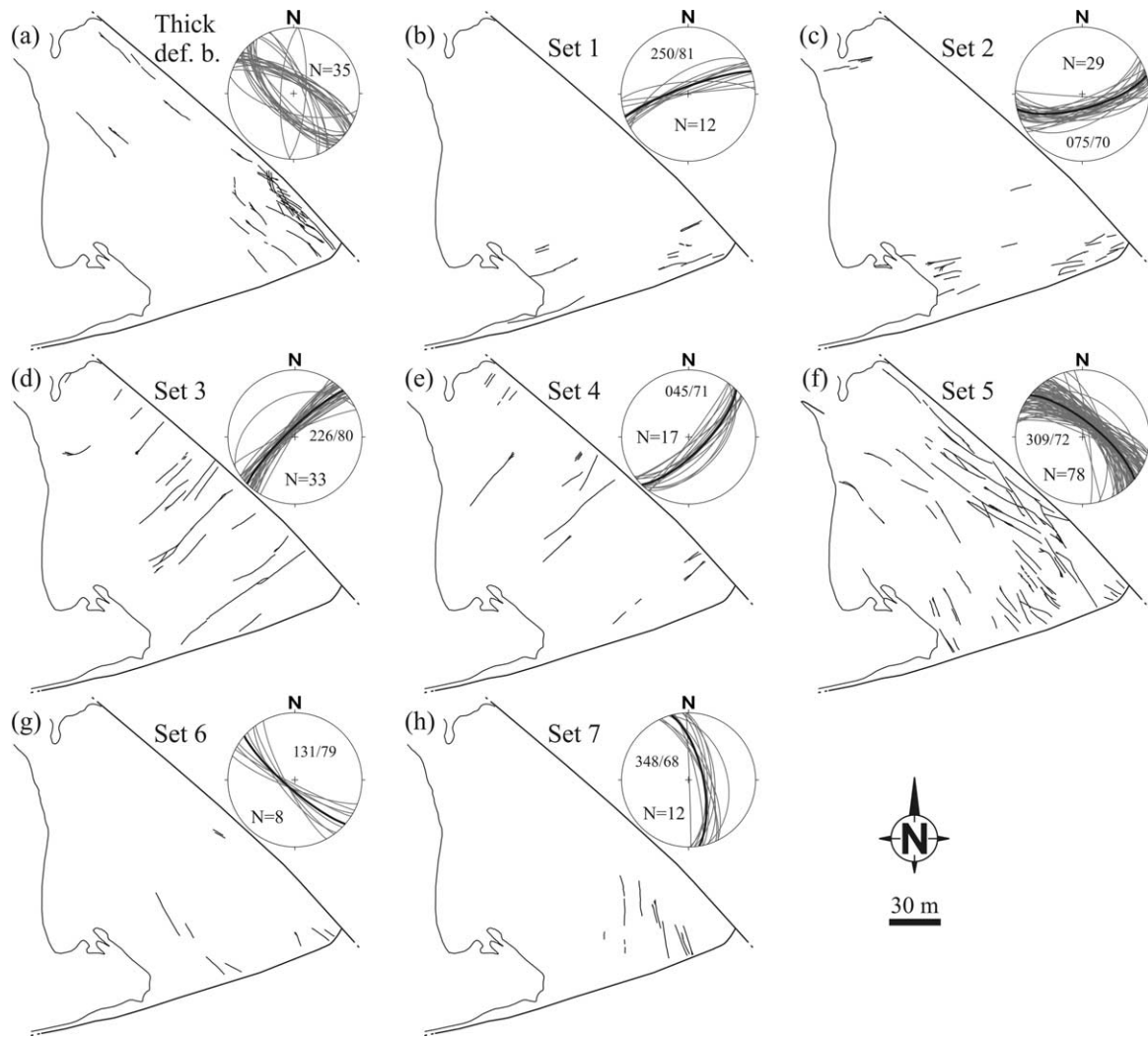
Fig. 12. Structural trends in the damage zone at the Courthouse Branch Point locality, and stereoplots (equal area, lower hemisphere) based on the structures delineated in Fig. 4. (a) Thick deformation bands. (b)–(h) Mainly thin deformation bands, slip surfaces and possibly some additional joints. Note the average plane (thick black line) and the average orientation in the stereoplots.

indurated as a result of quartz diagenesis prior to deformation.

Our findings do rule out the possibility that quartz diagenesis may have preceded or occurred simultaneously with formation of the thick deformation bands. For instance, Garden et al. (2001) reported minor quartz overgrowth in connection with pre-faulting diagenesis in sandstones along the Moab Fault. However, the temporal relations presented here suggest extensive quartz diagenesis between the formation of the thick and thin deformation bands.

Dissolved quartz grain contacts within the carbonate concretions (Fig. 5e) indicate that carbonate cementation postdates quartz diagenesis at the Courthouse Branch Point locality. Similar relations are also observed within the carbonate cemented wall rock that locally mantles dilated joints and slip surfaces.

Temporal relations between carbonate cementation and joint formation are composite. Differences in the optical orientation of carbonate precipitated inside dilated joints

and in the adjacent wallrock (Fig. 10c), suggest that carbonate cementation preceded and succeeded jointing. Also, the carbonate cemented sandstone that mantles many of these joints suggests that at least some carbonate cementation postdates jointing.

4.9. Frequency and distribution

The frequency of the various deformation structures at the Courthouse Branch Point locality was recorded along the 21 NS-oriented scan-lines in 1 m bins, and 1.75 km of scan-lines were recorded altogether. The scan-lines are not perpendicular to the main faults, but their orientation is not considered to have significantly biased the structural frequency data. Map displays of lateral frequency variations were generated by contouring the frequency data at specified intervals. The main structural trends and orientations (Fig. 4) were incorporated and used as a guide for contouring.
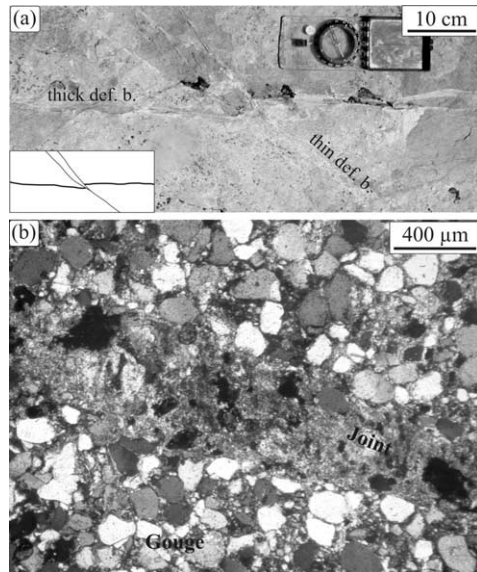
Fig. 13. (a) Thin deformation bands offset and postdate thick deformation bands. (b) A carbonate filled joint formed in carbonate cemented gouge indicates that the joints postdate the deformation bands. Photo locations are shown in Fig. 4.

The thick deformation bands show a preferred spatial association with Segment A, evident by an increase in frequency towards Segment A (Fig. 16a), but also by their parallelism with Segment A (Fig. 12a).

Thin deformation bands and associated slip surfaces and joints are compiled in a single structure frequency map (Fig. 16b). Distinguishing joints from the other structures in Fig. 16b was considered unattainable, due to the extensive amount of data and the difficulties and efforts involved in identifying joints in the field. Although joints have been observed, the quality of the structure frequency data is not good enough to render the spatial distribution of joints in a separate map. Nonetheless, our observations suggest that the thin deformation bands and slip surfaces are predominant and widely distributed within the damage zone, whereas joints are much less frequent, with the exception of local joint networks adjacent to Segment B. As such, the structure frequency map presented in Fig. 16b is considered to approximate the distribution of thin deformation bands and associated slip surfaces on the outcrop. The highest concentrations of these structures occur in the vicinity of the main fault segments and in particular along Segment B.
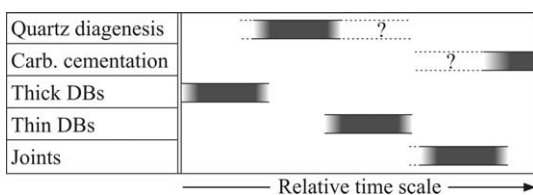

Fig. 14. Overview of timing relations between diagenetic and structural events based on observations from the Courthouse Branch Point outcrop.
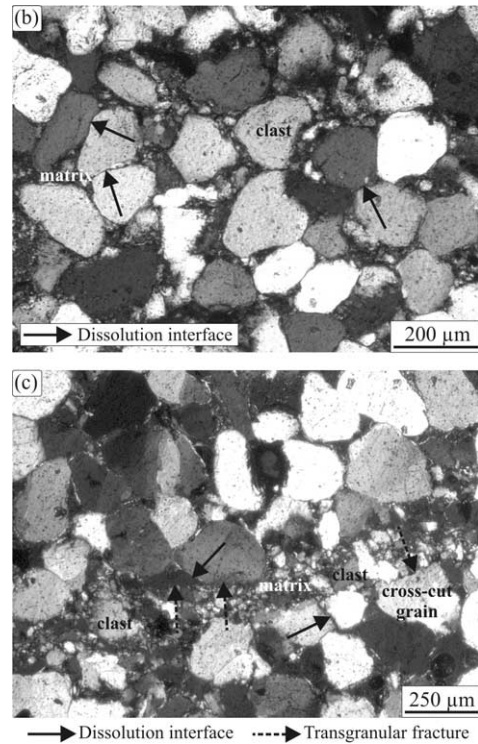

Fig. 15. Timing relations between quartz diagenesis and formation of thick and thin deformation bands. (a) Extensive quartz diagenesis sub-sequent to formation of thick deformation bands is indicated by dissolution interfaces at the contact between clasts and undeformed grains inside the thick deformation bands. (b) Cross-cut quartz grains and dissolution interfaces along the sidewall of thin deformation bands suggests that quartz diagenesis pre-dates the formation of these structures. See Fig. 4 and Table 1 for location and details.

5. Interpretation and discussion

5.1. Growth of thick deformation bands

The classical model of Aydin and Johnson (1978) on faulting in porous sandstones invokes a strain hardening mechanism for the development of deformation bands. Strain hardening causes shearing along a single deformation band to come to an end as strain delocalizes to the adjacent wallrock where a new deformation band nucleates. This sequence may repeat until a tabular zone of deformation bands has formed. Discrete slip surfaces may eventually develop along or within the deformation band zone. The deformation mechanism associated with the *thick* deformation bands in the Courthouse area appears to comply with this model, as indicated by the thickness of the individual bands and due to the fact that single thick bands do not develop slip surfaces.

5.2. Growth of thin deformation bands

Examination of thin sections has established the mechanism involved in the formation of the thin deformation bands as well as the kinematic relationship between
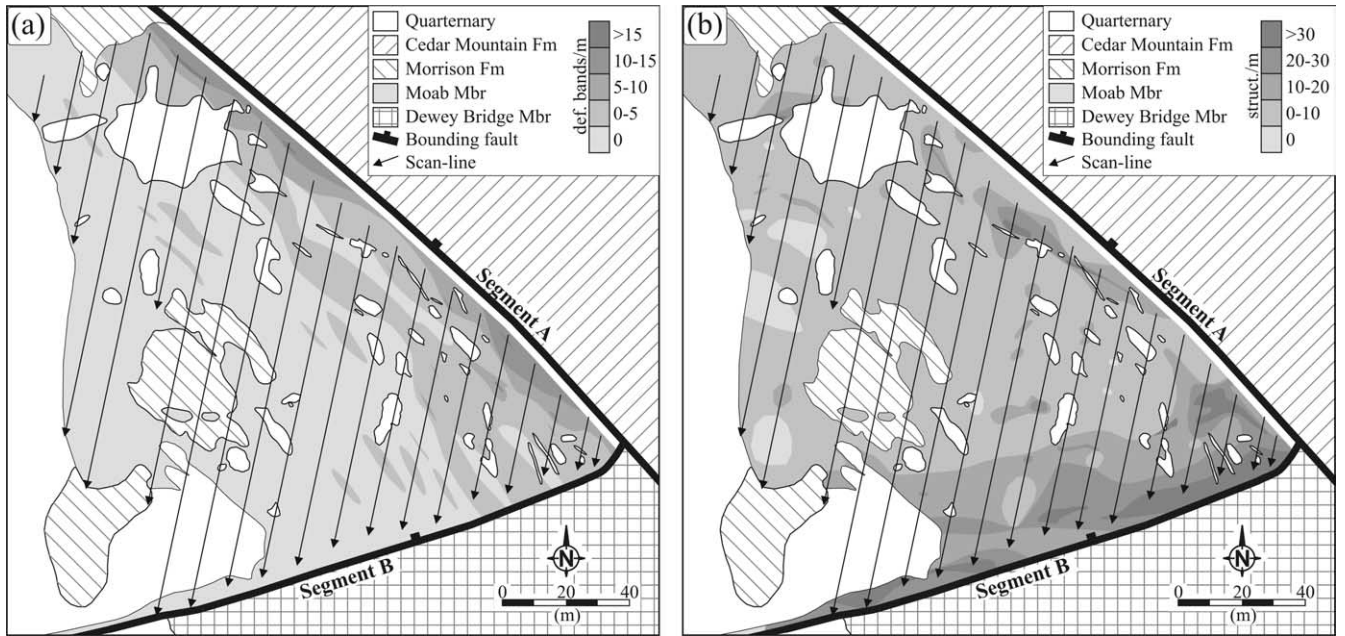
Fig. 16. (a) Spatial distribution of thick deformation bands in the damage zone at the Courthouse Branch Point locality. (b) Spatial distribution of thin deformation bands, slip surfaces and joints in the damage zone at the Courthouse Branch Point locality.

the thin deformation bands and the associated slip surfaces. Induration through quartz diagenesis, and locally carbonate cementation, affected the host rock prior to the formation of the thin deformation bands by increasing the cohesive strength of the grain contacts. Based on observations of the tip of the thin deformation band in Fig. 8 we argue that cohesive grain contacts inhibited grain reorganization, and for that reason the rock failed ultimately by cataclasis. Increased loading at the contact between the interconnected grains in response to shear caused intra-granular and trans-granular cracks to nucleate (Fig. 17a). Coalescence of these cracks lead to shear localization and formation of gouge, which, during the initial increments of shearing contained mostly larger clasts and minor matrix (Fig. 17b). Intense cataclasis produced a fine-grained matrix-supported quartz gouge and a throughgoing deformation band (Fig. 17c). Increased offset resulted in localization of narrow (10–20 μm) zones of extremely fine-grained gouge within the

thin deformation bands (Fig. 17d). Several of these fine-grained gouge zones have been observed in the extension of the tip of micro-fractures (Fig. 9c), which we interpret as minor slip patches. As such, we suggest that these slip patches nucleated within the most fine-grained gouge and that further propagation and linkage eventually produced mesoscale throughgoing slip surfaces (Fig. 17e).

Formation of the thin deformation bands was accommodated by intense cataclasis and matrix-dominated gouge developed at very low (≪0.5 mm) offsets. Our findings suggest that cataclasis was most intense during initial shear and then leveled off as the gouge became more matrix-dominated and attained better sorting with fewer clasts. Experimental studies on the growth of cataclastic deformation bands in porous sandstones have shown that the grains are rapidly reduced to a certain size, after which continued shear is accommodated mainly by rotation and translation of the grain fragments with limited grain
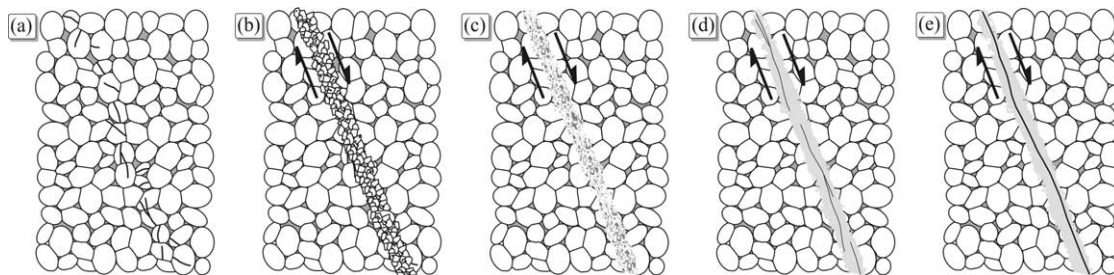

Fig. 17. Model of the formation of thin deformation bands and slip surfaces in the Moab Member at the Courthouse Branch Point locality. (a) Incipient shearing caused intra-granular cracks to nucleate in response to increased loading at the grain contacts. (b) Grain comminution results in formation of gouge, which initially contained predominantly larger clasts and minor matrix. (c) Intense cataclasis produced a fine-grained matrix-supported gouge and throughgoing deformation band. (d) The finest gouge localized along narrow (10–20 μm wide) zones, here rendered as solid black lines. (e) Microscopic slip patches nucleated within the finest gouge. Coalescence of several slip patches eventually lead to the formation of a continuous slip surface.

comminution (Engelder, 1974; Marone and Scholtz, 1989; Mair et al., 2000; Hadizadeh and Johnson, 2003). Hence, once matrix starts to dominate the gouge, cataclasis becomes gradually less important in the deformation process. The study of Marone and Scholtz (1989) on particle size distribution within simulated fault gouge indicates that cataclasis and grain size reduction in matrix-supported gouge preferentially affects larger clasts as they come into contact during deformation. Small grain fragments are less prone to fail. This result seem to be consistent with the development of the thin deformation bands where gouge along the most matured bands is dominantly very fine-grained (<10 μm) and contains very few large clasts.

Steen and Andresen (1999) described a series of cataclastic deformation bands that formed in carbonate cemented low porosity (<4%) sandstones. These deformation bands feature extensive grain comminution and exhibit a sharp boundary between the pristine host rock and the gouge zone, which penetrates the grains and the cement. It turns out that these morphological characteristics resemble those of the thin deformation bands examined at the Courthouse Branch Point. By investigating the tip of these bands Steen and Andresen (1999) also found that cataclasis was dominant already during the first increments of strain. They suggested, in agreement with our assumptions on the growth of the thin deformation bands, that strain hardening was not significant for the development of these structures.

The experimental gouge examined by Mair et al. (2000) exhibits a fractal grain size distribution and therefore compacts more efficiently compared with well-sorted gouge. It was inferred that compaction, in addition to the increase in the number of grain contacts during shear, provided a potential strain hardening mechanism for the development of their gouge strings. The presence of zones of thin deformation bands as described in the current study indicates strain hardening during their formation. However, slip patches along these structures also manifest the importance of strain softening during shear. Comparison between the microstructure of the thin deformation bands and the gouge strings of Mair et al. (2000) suggests that the gouge inside our thin deformation bands is much better sorted and contains significantly fewer large clasts. Hence, it appears that the nucleation of slip patches within the thin deformation bands was favored by more evenly distributed grain sizes and relatively good sorting. By comparison, zones of thick deformation bands exhibit poorly sorted gouge and shear was governed by strain hardening, rather than strain softening.

5.3. Influence of cementation and porosity

The coexistence of thin and thick deformation bands in the same rock calls for a change in physical conditions during deformation. Thick deformation bands can only form

in porous media, as the collapse of pore space is fundamental to the deformation process involved (Aydin and Johnson, 1978; Antonellini et al., 1994; Fowles and Burley, 1994). The formation of different types of deformation bands appears to depend on a large number of factors, including sorting, grain roundness, mineralogy, burial depth (lithostatic pressure), cementation, and local stress field (e.g. Antonellini and Pollard, 1995; Menéndez et al., 1996; Mair et al., 2000; Hesthammer and Fossen, 2001). Much research remains in order to understand the relative importance and interaction of these variables.

The interaction of Segment B with Segment A indicates that they formed more or less simultaneously (see below). This leaves us with the possibility that either changes in lithologic properties, such as porosity and/or cementation of grain contacts, or changes in the local stress state resulted in the different structural expression at a small scale. Davatzes and Aydin (2003) favored local deviations in the stress field as the most important reason why (thick) deformation bands and related faults coexist with what they refer to as joints and faulted joints. Our observations indicate to us that the change in porosity that has taken place in the rock may be the factor controlling the change from the formation of thick to thin deformation bands at the Courthouse Branch Point locality.

The Moab Member has a maximum porosity in the order of 20–25% (Antonellini and Aydin, 1994). The porosity of the Moab Member at the Courthouse Branch Point locality varies on a local scale from up to 17% in small volumes of pristine rock down to less than 1% in calcite concretions and zones of extensive quartz dissolution and precipitation. From what we know about the formation and growth of fractures versus deformation bands in sandstone a change in porosity from 20–25% to as low as 1% or less is significant (e.g. Wong et al., 1997; Steen and Andresen, 1999; Fisher et al., 2003). For instance, shear fractures are well developed in well-cemented and low (<5%) porosity sandstones of the Morrison Formation a few meters above the Moab Member in the Courthouse area, and deformation bands (thick or thin) are completely absent here.

We consider the thin deformation bands to represent a transitional structure between the thick deformation bands and shear fractures. They are more localized and involve higher strains than thick deformation bands, but still are not discrete shear fractures. Neither do they develop the relatively large (meter-scale) offsets accumulated on most slip surfaces, indicating that strain hardening may still be important. We suggest that the thin deformation bands formed in a sandstone that was at a physical transition between faulting and formation of deformation bands, controlled by reduction in porosity.

Flodin et al. (2003) examined the petrophysical constraints on contrasting deformation styles in eolian sandstones that have witnessed an identical deformation history. They noted that well cemented low-porosity sandstone had deformed predominantly by jointing, whereas

deformation band faulting prevailed in poorly cemented high porosity sandstone. Flodin et al. (2003) found that the contrast in deformation style was controlled by porosity and speculated that pore filling cements inhibited the formation of deformation bands. Reduction of porosity due to cementation causes an increase in the strength of granular rocks, such as sandstones, in particular when cement precipitates at grain contacts. Cements may increase the grain contact area, yielding a more uniform contact stress distribution, and thus provide less potential for intragranular failure (Yin and Dvorkin, 1994). Cement at grain contacts also generates more cohesive grain contacts, which prevent gliding and rotation of the grains (Bernabé et al., 1992). We consider cementation and grain dissolution to have a similar effect on the bulk rock strength. It follows that well cemented low-porosity rocks should favor limited grain reorganization during failure, which is consistent with our observations of thin deformation bands. Fault-related diagenetic activity strengthened the host rock (Moab
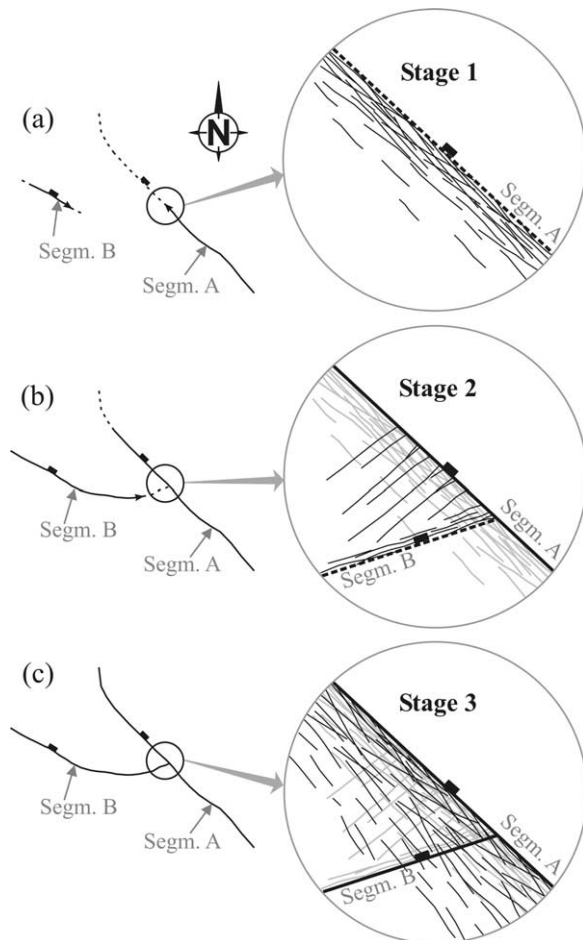

Fig. 18. Evolutionary model of the Courthouse Branch Point. Arrows on fault trace indicate direction of propagation. (a) Stage 1: Thick deformation bands formed prior to linkage in association with faulting along Segment A. The main event of the quartz diagenesis occurred between stages 1 and 2. (b) Stage 2: linkage between Segments A and B produced structural trends that abut Segment A at high angles. (c) Stage 3: formation of new structures parallel to Segment A.

Member) so that nucleation of thin deformation bands probably required higher differential stress compared with the thick deformation bands. This may explain the intensity of the cataclasis associated with the thin deformation bands.

5.4. Relative timing of quartz cementation and faulting

The porosity structure of the Moab Member adjacent to the Courthouse Branch Point changed during the course of the deformation, probably through the circulation of hot fluids on Segments A and B. Evidence of fluid circulation is manifested not only by carbonate and ore mineralization listed by Foxford et al. (1996), but also by quartz cementation in the damage zone of the main faults. Quartz cementation along Segment A in the Courthouse area has locally turned the sandstone into a quartzite. The quartzite has preserved the anastomosing network of densely packed thick deformation bands, showing that the thick deformation bands along this fault formed at an early stage. Hence, Segment A developed according to the model presented by Aydin and Johnson (1978). Segment B, on the other hand, does not show evidence of an early stage of (thick) deformation band formation. This may indicate that Segment B connected to Segment A at a later stage, i.e. after Segment A was established, but during continued slip along Segment A, and during or shortly after quartz cementation of the Moab Member. Several lines of evidence are consistent with this interpretation:

1. Segment B curves from the general NW–SE trend to a more E–W trend as it approaches Segment A (Fig. 1). Segment A itself seems, however, to be completely unaffected by Segment B as far as orientation and geometry are concerned.
2. The displacement of Segment B decreases towards Segment A (Foxford et al., 1996). This indicates that Segment B grew towards Segment A rather than out of Segment A.
3. Segment B does not cross-cut Segment A. All of these geometric characteristics indicate that Segment B was influenced by the already existing Segment A at the time.
4. Thick deformation bands are only developed along Segment A at the Courthouse Branch Point (Figs. 4, 12a and 16a), not along Segment B.
5. Thin deformation bands and slip surfaces are concentrated along both Segment B and Segment A (Fig. 16b), but cross-cutting relationships suggest that the trends that align with Segment B predate trends parallel to Segment A.

5.5. Evolutionary model

Based on the observations made in this study we propose a three-stage evolutionary model (Fig. 18) for the formation

of the fault damage zone in the Moab Member at the Courthouse Branch Point locality.

Stage 1 (Fig. 18a) describes the northwestward growth of Segment A associated with the formation of sub-parallel thick deformation bands prior to linkage with Segment B. Since deformation bands at least in part form in the process zone ahead of a propagating fault tip (e.g. Shipton and Cowie, 2001), and since deformation bands themselves do not act as pathways for fluids, the thick deformation bands are believed to have formed prior to fluid-assisted quartz cementation of the Moab Member. Fault-assisted cementation is likely to have commenced as soon as Segment A possessed slip surfaces capable of transmitting fluids to the Courthouse Branch Point locality.

Stage 2 (Fig. 18b) demonstrates the origin of the Courthouse Branch Point by the growth of Segment B toward Segment A. At the time when Segment B entered the damage zone of Segment A, formation of thick deformation bands had ceased and thin deformation bands, slip surfaces, and possibly joints formed at high angles to Segment A accompanying porosity reduction. These structures are oriented along two sub-trends that deviate at an angle of approximately 20°. The sub-trend oriented normal to Segment A persists far into the damage zone and its orientation is in keeping with the direction of the least compressive principal stress, as predicted from numerical modeling of stress perturbations around the Courthouse Branch Point (Davatzes et al., 2005). The other sub-trend localizes along Segment B.

Stage 3 (Fig. 18c) illustrates the situation subsequent to linkage. Faulting along Segment A leads to the formation of sub-parallel thin deformation bands and slip surfaces that cross-cut structures oriented perpendicular to Segment A. Faulting along Segment B appears to have been localized to the fault core and did not affect the damage zone to any essential extent.

Field observations of cross-cutting relationship between the different structural trends have shown no simultaneous growth of structures either parallel or perpendicular to Segment A. This finding leaves us with two possibilities: Segment A was either inactive or faulting was localized to the core during stage 2. If Segment A was active during stage 2, it may have continued to propagate farther to the NW, completely unaffected by the stress perturbations around Segment B (see discussion above). Alternatively, the tip of Segment A had reached its present position already at the end of stage 1 and faulting in stage 2 was constrained to the accumulation of displacement on the fault core without further lateral expansion to the NW.

5.6. Discussion of alternative models

Davatzes and Aydin (2003) and Davatzes et al. (2005) recognized two different groups of structures associated with different deformation mechanisms, which was accounted for by a change of stress state from compressive stress to locally effective tensile stresses. In their view, deformation bands, deformation band zones and associated slip surfaces occur everywhere along the fault zone and are the product of localized cataclastic shear failure. Joints, sheared joints and breccia localize at intersections and relays that accommodate extension, i.e. reduction of the local compressive stress, and consistently overprint the deformation bands. Fault formation from shearing of joints requires first the nucleation of joints due to local tensile stresses, followed by local stress rotation and shearing across the weak joint plane. Davatzes et al. (2005) suggest also that mechanical interaction between Segments A and B is the main control on the structural heterogeneity (architecture) in the Courthouse area.

While local changes in the state of stress is expected along slipping faults, the model of Davatzes et al. (2005) is inconsistent with our observations. We identify numerous thin deformation bands where Davatzes et al. (2005) report joints and faulted joints. Evidence from photomicrographs of the thin deformation bands suggests that these structures nucleated and grew ultimately by cataclasis (Figs. 7b–d and 8) in response to shearing and are therefore unlikely to be faulted joints. In addition, our observation of slip patches along the thin deformation bands suggests that they locally developed into slip surfaces or minor faults (Fig. 9) and thus represent faulted deformation bands rather than faulted joints. According to our observations, these structures formed by shearing, and not as mode I fractures, which suggests that they do not fit the numerical and conceptual model proposed by Davatzes et al. (2005).

This is not conclusive evidence that local stress perturbations associated with slip across the two fault segments did not play a role in the formation of the composite damage zone in the Courthouse area, and there are joints and thin deformation bands with anomalous orientations in this area that may be explained by a stress perturbation model. We believe, however, that the change from thick to thin deformation bands identified in this paper can be better explained by the reduction of porosity through diagenetic processes related to circulation of fluids along the faults.

6. Conclusions

The damage zone around the Courthouse Branch Point exhibits a composite pattern of small-scale deformation structures with contrasting deformation mechanisms and a wide range of orientations. Detailed field examination has shown that thick deformation bands first formed along the trend of Segment A, followed by thinner (0.1–0.2 mm) deformation bands that parallel both the main segments and abut against and normal to Segment A.

The thick deformation bands are about 1–1.5 mm wide, show moderate cataclasis and typically cluster in zones, suggesting that shear was associated with strain hardening.

The thin deformation bands formed ultimately by cataclasis, which produced a fine gouge at relatively low offsets. These structures locally cluster in densely packed zones or form slip surfaces, indicating that both strain hardening and strain softening mechanisms were involved during shear.

The change from thick to thin deformation bands is correlated with a period of quartz precipitation and dissolution that reduced the pore space after the thick deformation bands formed. We argue that reduction of porosity may have increased the cohesive strength of the grain contacts and thus restricted grain reorganization by rotation and sliding during shear. Quartz diagenesis is ascribed to interaction of hot fluids flushing through the fault zone.

This study shows that where syn-kinematic diagenesis has occurred during fault development and growth in porous sandstones, the properties of the damage zone of one fault do not necessarily correspond to those of a neighboring fault in the same fault array and lithological unit. Clearly, more field observations and experimental work are needed to better understand how changes in porosity and related factors influence the resulting deformation structures and mechanisms in porous media.

Acknowledgements

References

Antonellini, M.A., Aydin, A., 1994. Effect of faulting on fluid flow in porous sandstones: petrophysical properties. American Association of Petroleum Geologists Bulletin 78, 355–377.

Antonellini, M.A., Pollard, D.D., 1995. Distinct element modeling of deformation bands in sandstone. Journal of Structural Geology 17 (8), 1165–1182.

Antonellini, M.A., Aydin, A., Pollard, D.D., 1994. Microstructure of deformation bands in porous sandstones at Arches National Park, Utah. Journal of Structural Geology 16, 941–959.

Aydin, A., 1978. Small faults formed as deformation bands in sandstone. In: Byerlee, J.D., Wyss, M. (Eds.), Rock Friction and Earthquake Prediction Pure and Applied Geophysics, 116, pp. 913–930.

Aydin, A., Johnson, A.M., 1978. Development of faults as zones of deformation bands and as slip surfaces in sandstone. In: Byerlee, J.D., Wyss, M. (Eds.), Rock Friction and Earthquake Prediction Pure and Applied Geophysics, 116, pp. 931–942.

Bernabé, Y., Fryer, D.T., Hayes, J.A., 1992. The effect of cement on the strength of granular rocks. Geophysical Research Letters 19 (14), 1511–1514.

Cruikshank, K.M., Zhao, G., Johnson, A.M., 1991. Analysis of minor fractures associated with joints and faulted joints. Journal of Structural Geology 13, 865–886.

Davatzes, N.C., Aydin, A., 2003. Overprinting faulting mechanisms in high porosity sandstones of SE Utah. Journal of Structural Geology 25, 1795–1813.

Davatzes, N.C., Eichhubl, P., Aydin, A., 2005. The structural evolution of fault zones in sandstone by multiple deformation mechanisms; Moab fault, SE Utah. Geological Society of America Bulletin 117 (1), 135–148.

Doelling, H.H., 1988. Geology of Salt Valley Anticline and Arches National Park, Grand County, Utah. In: Doelling, H.H., Oviatt, C.G., Huntoon, P.W. (Eds.), Salt Deformation in the Paradox Region Bulletin, 122. Utah Geological and Mineral Survey, Salt Lake City, UT, pp. 1–58.

Doelling, H.H., 2000. Geology of Arches National Park, Grand County, Utah. In: Sprinkel, D.A., Chidsey Jr., T.C., Anderson, P.B. (Eds.), Geology of Utah's Parks and Monuments. Utah Geological Association, Salt Lake City, UT, United States, pp. 11–36.

Doelling, H.H., 2001. Geologic map of the Moab and eastern part of the San Rafael Desert 30′ × 60′ quadrangles, Grand and Emery Counties, Utah, and Mesa County, Colorado. Utah Geological Survey Map 180, scale 1:100,000.

Du Bernard, X., Eichhubl, P., Aydin, A., 2002. Dilation bands: a new form of localized failure in granular media. Geophysical Research Letters 29, 2176–2179.

Dunn, D.E., LaFountain, L., Jackson, R.E., 1973. Porosity dependence and mechanism of brittle fracture in sandstones. Journal of Geophysical Research 78, 2403–2417.

Engelder, J.T., 1974. Cataclasis and the generation of fault gouge. Geological Society of America Bulletin 85 (10), 1515–1522.

Fisher, Q.J., Casey, M., Harris, S.D., Knipe, R.J., 2003. Fluid flow properties of faults in sandstone: the importance of temperature history. Geology 31 (11), 965–968.

Flodin, E., Prasad, M., Aydin, A., 2003. Petrophysical constraints on deformation styles in Aztec Sandstone, southern Nevada, USA. Pure and Applied Geophysics 160, 1589–1610.

Fossen, H., Hesthammer, J., 1997. Geometric analysis and scaling relations of deformation bands in porous sandstone from the San Rafael Desert, Utah. Journal of Structural Geology 19, 1479–1493.

Fowles, J., Burley, S., 1994. Textural and permeability characteristics of faulted, high porosity sandstones. Marine and Petroleum Geology 11, 608–623.

Foxford, K.A., Garden, I.R., Guscott, S.C., Burley, S.D., Lewis, J.L.L., Walsh, J.J., Watterson, J., 1996. The field geology of the Moab Fault. In: Huffman, A.C., Lund, W.R.J., Godwin, L.H. (Eds.), Geology and Resources of the Paradox Basin, 25. Utah Geological Association Guidebook, pp. 265–283.

Garden, I.R., Guscott, S.C., Burley, S.D., Foxford, K.A., Walsh, J.J., Marshall, J., 2001. An exhumed palaeo-hydrocarbon migration fairway in a faulted carrier system, Entrada Sandstone of SE Utah, USA. Geofluids 1 (3), 195–213.

Hadizadeh, J., Johnson, W.K., 2003. Estimating local strain due to comminution in experimental cataclastic textures. Journal of Structural Geology 25 (11), 1973–1979.

Hesthammer, J., Fossen, H., 2000. Uncertainties associated with fault sealing analysis. Petroleum Geoscience 6, 37–45.

Hesthammer, J., Fossen, H., 2001. Structural core analysis from the Gullfaks area, northern North Sea. Marine and Petroleum Geology 18 (3), 411–439.

Hesthammer, J., Bjorkum, P.A., Watts, L., 2002. The effect of temperature on sealing capacity of faults in sandstone reservoirs; examples from the Gullfaks and Gullfaks Sor fields, North Sea. American Association of Petroleum Geologists Bulletin 86, 1733–1751.

Huntoon, P.W., 1988. Late Cenozoic gravity tectonic deformation related to the Paradox salts in the Canyonlands area of Utah. In: Doelling, H.H., Oviatt, C.G., Huntoon, P.W. (Eds.), Salt Deformation in the Paradox Region Bulletin, 122. Utah Geological and Mineral Survey, Salt Lake City, UT, pp. 79–93.

Knipe, R.J., Fisher, Q.J., Jones, G., Clennel, M.B., Farmer, A.B., Harrison, A., Kidd, B., McAllister, E., Porter, J.R., White, E.A., 1997. Fault seal analysis: successful methodologies, application and

future directions. In: Moller-Pedersen, P., Koestler, A.G. (Eds.), Hydrocarbon Seals: Importance for Exploration and Production, 7. Norwegian Petroleum Society Special Publication, pp. 15–40.

Mair, K., Main, I., Elphick, S., 2000. Sequential growth of deformation bands in the laboratory. Journal of Structural Geology 22, 25–42.

Marone, C., Scholz, C.H., 1989. Particle-size distribution and microstructures within simulated fault gouge. In: Spray, J.G., Hudleston, P.J. (Eds.), Friction Phenomena in Rock Journal of Structural Geology, 11. Pergamon, Oxford and New York, pp. 799–814. International.

Menéndez, B., Zhu, W., Wong, T.F., 1996. Micromechanics of brittle faulting and cataclastic flow in Berea Sandstone. Journal of Structural Geology 18 (1), 1–16.

Mollema, P.N., Antonellini, M.A., 1996. Compaction bands: a structural analog for anti-mode I cracks in aeolian sandstone. Tectonophysics 267, 209–228.

Nuccio, V.F., Condon, S.M., 1996. Burial and Thermal History of the Paradox Basin, Utah and Colorado, and Petroleum Potential of the Middle Pennsylvanian Paradox Basin. US Geological Survey, Reston, VA, USA.

O'Sullivan, R.B., 1981. Stratigraphic sections of Middle Jurassic Entrada Sandstone and related rocks from Salt Valley to Dewey Bridge in east-central Utah. US Geological Survey Oil and Gas Investigations Chart OC-113.

Oviatt, C.G., 1988. Evidence for quaternary deformation in the Salt Valley Anticline, southeastern Utah. In: Doelling, H.H., Oviatt, C.G., Huntoon, P.W. (Eds.), Salt Deformation in the Paradox Region Bulletin, 122. Utah Geological and Mineral Survey, Salt Lake City, UT, pp. 61–76.

Reches, Z., Lockner, D.A., 1994. Nucleation and growth of faults in brittle rocks. Journal of Geophysical Research, B, Solid Earth and Planets 99, 18159–18174.

Shipton, Z.K., Cowie, P.A., 2001. Damage zone and slip-surface evolution over μm to km scales in high-porosity Navajo Sandstone, Utah. Journal of Structural Geology 23 (12), 1825–1844.

Shipton, Z.K., Cowie, P.A., 2003. A conceptual model for the origin of fault damage zone structures in high-porosity sandstone. Journal of Structural Geology 25, 333–344.

Steen, O., Andresen, A., 1999. Effects of lithology on geometry and scaling of small faults in Triassic sandstones, East Greenland. Journal of Structural Geology 21 (10), 1351–1368.

Stevenson, G.M., Baars, D.L., 1986. The Paradox; a pull-apart basin of Pensylvanian age. American Association of Petroleum Geologists Memoir 41, 513–539.

Underhill, J.R., Woodcock, N.H., 1987. Faulting mechanisms in high-porosity sandstones; New Red Sandstone, Arran, Scotland. In: Jones, M.E., Preston, M.F. (Eds.), Deformation of Sediments and Sedimentary Rocks, 29. Geological Society Special Publications, pp. 91–105.

Wilson, J.E., Goodwin, L.B., Lewis, C.J., 2003. Deformation bands in nonwelded ignimbrites; petrophysical controls on fault-zone deformation and evidence of preferential fluid flow. Geology (Boulder) 31, 837–840.

Wong, T.f., David, C., Zhu, W., 1997. The transition from brittle faulting to cataclastic flow in porous sandstones; mechanical deformation. Journal of Geophysical Research, B, Solid Earth and Planets 102 (2), 3009–3025.

Yin, H., Dvorkin, J., 1994. Strength of cemented grains. Geophysical Research Letters 21 (10), 903–906.

Zhao, G., Johnson, A.M., 1992. Sequence of deformations recorded in joints and faults, Arches National Park, Utah. Journal of Structural Geology 14, 225–236.